

# CHEMICAL CONSTRAINTS ON THE CONTRIBUTION OF POPULATION III STARS TO COSMIC REIONIZATION

GIRISH KULKARNI<sup>1</sup>, JOSEPH F. HENNAWI<sup>1</sup>, EMMANUEL ROLLINDE<sup>2</sup>, ELISABETH VANGIONI<sup>2</sup>

*Draft version February 26, 2018*

## ABSTRACT

Recent studies have highlighted that galaxies at  $z = 6-8$  fall short of producing enough ionizing photons to reionize the IGM, and suggest that Population III stars could resolve this tension, because their harder spectra can produce  $\sim 10\times$  more ionizing photons than Population II. But this argument depends critically on the duration of the Population III era, and because Population III stars form from pristine gas, in turn depends on the rate of galactic enrichment. We use a semi-analytic model of galaxy formation which tracks galactic chemical evolution, to gauge the impact of Population III stars on reionization. Population III SNe produce distinct metal abundances, and we argue that the duration of the Population III era can be constrained by precise relative abundance measurements in high- $z$  damped Ly $\alpha$  absorbers (DLAs), which provide a chemical record of past star-formation. We find that a single generation of Population III stars can self-enrich galaxies above the critical metallicity  $Z_{\text{crit}} = 10^{-4}Z_{\odot}$  for the Population III-to-II transition, on a very short timescale  $t_{\text{self-enrich}} \sim 10^6$  yr, owing to the large metal yields and short lifetimes of Population III stars. This subsequently terminates the Population III era, hence they contribute  $\gtrsim 50\%$  of the ionizing photons only for  $z \gtrsim 30$ , and at  $z = 10$  contribute  $< 1\%$ . The Population III contribution can be increased by delaying metal mixing into the ISM. However comparing the resulting metal abundance pattern to existing measurements in  $z \lesssim 6$  DLAs, we show that the fractional contribution of high-mass Population III stars to the ionization rate must be  $\lesssim 10\%$  at  $z = 10$ . Future abundance measurements of  $z \sim 7-8$  QSOs and GRBs should probe the era when the chemical vestiges of Population III star formation become detectable.

*Subject headings:* Cosmology: dark ages, reionization, first stars — galaxies: evolution — galaxies: ISM — stars: Population III

## 1. INTRODUCTION

Reionization of the intergalactic medium (IGM) is a watershed event in the history of the universe, and is tightly coupled to the problem of galaxy formation at high redshift. The primary evidence for hydrogen reionization comes from observation of Gunn-Peterson troughs (Gunn & Peterson 1965) in spectra of high-redshift quasars (Fan et al. 2006b; Mortlock et al. 2011). Other pieces of evidence are in the angular power spectrum of polarization anisotropy of the CMB (Larson et al. 2011; Hinshaw et al. 2012), evolution of the IGM temperature (Hui & Haiman 2003; Becker et al. 2011; Raskutti et al. 2012), and evolution of the luminosity function of Lyman- $\alpha$  emitters (Ouchi et al. 2010). For a more complete discussion of observational constraints on reionization see, e.g., review by Fan et al. (2006a). A general picture that emerges from these observations and a broad class of theoretical models is that H I reionization was a gradual process that lasted for hundreds of Myr from  $z \sim 20$  to  $z \sim 6$ , and that star-forming galaxies most likely provided the required ionizing photons (Choudhury & Ferrara 2006; Mitra et al. 2011; Kuhlen & Faucher-Giguère 2012; Robertson et al. 2013).

Given this evidence, several recent studies have used averaged radiative transfer models to ask whether the

observed populations of galaxies at high redshift produce enough ionizing photons to reionize the IGM (Robertson et al. 2010). Kuhlen & Faucher-Giguère (2012) studied constraints from measurements of the hydrogen photoionization rate,  $\Gamma_{\text{HI}}$ , from the (post-reionization) Lyman- $\alpha$  forest (Faucher-Giguère et al. 2008; Becker & Bolton 2013) and the requirement that  $\Gamma_{\text{HI}}$  should evolve in a continuous manner through the epoch of reionization. They concluded these two conditions require either a rapid evolution in the ionizing photon escape fraction,  $f_{\text{esc}}$ , or an extrapolation of the galaxy luminosity function to extremely faint luminosities ( $M_{\text{UV}} \sim -10$  or  $L \sim 0.002L_*$ ). Several independent studies have come to similar conclusions (Fontanot et al. 2012; Mitra et al. 2012; Finlator et al. 2012; Raskutti et al. 2012; Haardt & Madau 2012; Alvarez et al. 2012; Robertson et al. 2013). This work suggests that (1)  $f_{\text{esc}}$  is at least ten times higher at  $z = 10$  than at  $z = 4$ , and/or (2) there is a large population of undetected faint galaxies that produces the lion's share of the total ionizing flux, and/or (3) new galactic sources, such as mini-quasars or Population III stars, are active at high redshift and assist star-forming galaxies in reionizing the IGM.

Owing to their primordial composition, Population III stars have harder spectra and thus emit more hydrogen-ionizing photons. A cluster of Population III stars (with 100–260  $M_{\odot}$  Salpeter IMF) produces an order of magnitude more hydrogen-ionizing photons than a cluster of Population II stars (with 0.1–100  $M_{\odot}$  Salpeter IMF) with the same total mass (Schaerer 2002). Thus, if the

<sup>1</sup> Max Planck Institute for Astronomy, Königstuhl 17, 69117 Heidelberg, Germany; girish@mpia-hd.mpg.de

<sup>2</sup> Institut d'Astrophysique de Paris, UMR 7095, UPMC, Paris VI, 98 bis boulevard Arago, 75014 Paris, France

Population III star formation rate is high enough, their contribution to the total ionizing photon budget could be significant. In this paper, we study the impact of Population III stars on reionization using a semi-analytic model of galaxy formation that tracks galactic chemical evolution and is fully coupled to the evolution of the thermal and ionization state of the IGM. Tracking the chemical evolution is crucial for understanding the contribution of Population III stars, which in our model form when the gas-phase metallicity of interstellar media (ISM) of galaxies is below a critical metallicity  $Z_{\text{crit}}$ . It is these stars in the very first galaxies that presumably initiated the process of reionization as they were likely the first sources of hydrogen-ionizing photons. As the formation of these stars depends on the metallicity of the gas out of which they form, the total contribution of these stars to the cosmic star formation rate (SFR) density, and hence the ionizing photon budget, depends on the chemical evolution of their environment, which is precisely what our model aims to calculate.

The role of Population III stars in cosmic chemical and ionization evolution has been studied previously. Faced with a high value of the Thomson scattering optical depth to the last scattering surface,  $\tau_e$ , reported by the first-year WMAP results  $\tau_e = 0.17$  (Spergel et al. 2003), which suggested that reionization occurred very early, several studies considered the ionizing emissivity of Population III stars (Venkatesan et al. 2003; Wyithe & Loeb 2003; Cen 2003; Sokasian et al. 2004; Yoshida et al. 2004), and others considered reionization scenarios driven by Population III stars (Daigne et al. 2004; Choudhury & Ferrara 2005; Daigne et al. 2006; Rollinde et al. 2009; Mitra et al. 2011). Due to the widely different methods and assumptions of these works, it is not straightforward to compare their results. Nonetheless, there are some common features in their results. In all of these models, reionization is initiated by Population III stars, which dominate the cosmic stellar content for some time. Eventually, however, the Population III SFR is reduced due to chemical enrichment of the star-forming gas, and the process of reionization is completed by Population II stars. A general conclusion of these studies was that, under conservative assumptions regarding various feedback processes (chemical, star formation, photoionization), Population III stars could contribute significantly to hydrogen reionization at  $z \gtrsim 10$ .

However, none of these models track the chemical evolution of the galaxies that host Population III stars at high redshift.<sup>3</sup> This is a significant drawback, because the time-scale over which the ISM of these galaxies is enriched by the first generation of Population III stars directly regulates the cosmic Population III star formation rate and hence the contribution of Population III stars to reionization. Indeed, Wise et al. (2012) recently used radiation hydrodynamics simulations to argue for just this kind of feedback. These authors found that for high-mass Population III stars (Chabrier IMF with  $M_{\text{char}} = 100 M_{\odot}$ ), which produce pair-instability supernovae, just one supernova is enough to enrich the parent halo to a metal-

<sup>3</sup> Models of Population III star formation that implement chemical evolution exist in the literature (e.g., Salvadori et al. 2007). These have proven to be very useful in studying, e.g., the extremely metal-poor stars in the Galactic halo. But these models do not calculate IGM reionization history.

licity of  $10^{-3} Z_{\odot}$  and prevent further Population III star formation. However, these authors did not study the implications of this chemical feedback on the contribution of Population III star-forming haloes to ionizing photon budget and reionization. This would require simulating star formation and chemical feedback for a cosmic ensemble of haloes with a wide range of masses, and coupling these to the IGM via radiative transfer while considering various observational constraints on reionization.

To summarize, previous work aiming to understand the contribution of high-redshift faint galaxies or Population III star-forming galaxies to reionization (e.g. Venkatesan et al. 2003; Choudhury & Ferrara 2005; Robertson et al. 2013) did not consider the detailed physics of galaxy formation, with chemical evolution and Population III star formation, while models that included these effects (Salvadori et al. 2007; Wise et al. 2012) did not couple galaxy formation with IGM reionization. In Kulkarni et al. (2013) we presented a semi-analytic model of galaxy formation that tracks the chemical evolution of galaxies as well as the thermal and ionization evolution of the IGM, and used this model to argue that measurements of relative abundances in high-redshift Damped Ly $\alpha$  systems can place interesting constraints on the Population III IMF. In this paper, we use this model to study the impact of Population III star-formation on reionization. Our model improves upon previous work on this subject in three important ways. First, it accounts for chemical evolution within a halo in detail, as part of a semi-analytical model of galaxy formation, taking into account stellar lifetimes, and inflows and outflows. This lets us study the Population III-to-II transition in haloes of various masses. Second, it uses halo mass assembly histories from cosmological simulations and fully couples galaxy formation to the thermal and ionization evolution of the IGM. This also lets us consider halo-mass-dependent effects like photoionization feedback. Third, we consider a range of Population III IMFs that presumably bracket the true IMF. A chemical evolution model with these three features, coupled self-consistently with thermal and ionization evolution of the IGM, provides a useful framework to study the contribution of Population III stars to reionization.

## 2. MODELING THE COUPLED EVOLUTION OF GALAXIES AND THE IGM

We use a model of galaxy formation and IGM evolution described in Kulkarni et al. (2013). Here we highlight the main features of the model, and refer the reader to that paper for additional details.

1. Average mass assembly histories of dark matter haloes are obtained from fitting functions calibrated to cosmological simulations (Fakhouri et al. 2010) for a number of logarithmically spaced halo masses. These assembly histories are a function of halo mass at  $z = 0$ .
2. Baryonic evolution is implemented for each halo mass value. In simplest terms, this assumes that a halo (1) accretes baryons through cosmological accretion, (2) forms stars from any gas contained in the halo for sufficiently long duration, and (3) ejects baryons via supernova powered outflows.

- This lets us calculate various properties—such as metallicity and star formation rate—as functions of halo mass. Global averages, such as the cosmic SFR density, are calculated by integrating over all halo masses.
3. Gas content of a halo is influenced by gas inflow due to cosmic accretion, star formation, stellar mass loss, and gas outflow due to supernova feedback. Gas inflow is calculated as being proportional to the dark matter accretion rate as given by the mass assembly history. Outflow rates are calculated according to the stellar IMF employed, by comparing the kinetic energy released by supernovae with the depth of the halo potential well. We also account for stellar lifetimes and mass loss from existing stars.
  4. We assume that star formation rate,  $\psi$ , in a halo tracks the total amount of cold gas,  $M_{\text{cool}}$ , which is determined by defining a metallicity dependent cooling radius (Kauffmann et al. 1999; Springel & Hernquist 2003).
  5. Metal content of a halo is calculated by accounting for nucleosynthetic yields by integrating over the Population II and Population III stellar IMFs. Halo metallicity is diluted by inflows from the metal-poor IGM and is enhanced by stellar nucleosynthesis. We do not assume instantaneous recycling in this calculation, i.e., we fully account for the delay in the production of metals due to finite stellar lifetimes. In this work, our fiducial model assumes instantaneous and homogeneous mixing of metals in the ISM. But we also consider variations of the model which relax this assumption.
  6. We implement Population III stars using a critical metallicity argument  $Z_{\text{crit}}$ , with our fiducial value as  $Z_{\text{crit}} = 10^{-4} Z_{\odot}$ . When the ISM metallicity in a halo becomes larger than  $Z_{\text{crit}}$ , Population III star formation stops, and new stars form according to a Population II IMF.
  7. We consider two different Population III IMFs (Turk et al. 2009; Dopcke et al. 2011): 1–100  $M_{\odot}$  Salpeter and 100–260  $M_{\odot}$  Salpeter. These are selected to represent two extreme possibilities. (We discuss this choice below.) The Population II IMF is kept constant at 0.1–100  $M_{\odot}$  Salpeter.
  8. Stellar lifetimes are taken from Maeder & Meynet (1989) and Schaerer (2002). Metal yields are taken from Heger & Woosley (2002) and Woosley & Weaver (1995). Population II SEDs are synthesised using STARBURST99 (Leitherer et al. 1999; Vázquez & Leitherer 2005) with respective metallicities. Synthetic spectra of Population III stars are taken from Schaerer (2002).
  9. We model the thermal, ionization, and chemical evolution of the IGM by implementing an inhomogeneous IGM with a lognormal density distribution. We calculate the evolution of volume filling factor of H II regions,  $Q_{\text{HII}}(z)$ , according to the method outlined by Miralda-Escudé et al.

(2000). Reionization is said to be complete when all low-density regions are ionized (we denote the corresponding redshift of reionization by  $z_{\text{reion}}$ ). The corresponding IGM thermal evolution is determined by solving the thermal evolution equation (Chiu & Ostriker 2000; Hui & Haiman 2003), accounting for photoheating and Compton and recombination cooling. The minimum mass of star-forming regions is calculated from the IGM temperature using the Jeans criterion (Barkana & Loeb 2001). Chemical evolution of the IGM is calculated by accounting for outflows from haloes of all masses.

Before discussing our results, we briefly comment on the Population III IMFs considered in this work. The IMF of Population III stars is poorly understood. Several early studies predicted that Population III stars have a characteristic mass of a few hundred  $M_{\odot}$  (e.g., Abel et al. 2002). In recent years, this prediction has come down in the range of 20–100  $M_{\odot}$  (e.g., Turk et al. 2009). Recently, Dopcke et al. (2011) argued that in the absence of metal-line cooling, dynamical effects can still lead to fragmentation in proto-stellar gas clouds. In their simulations, this resulted in Population III stars with masses as low as 0.1  $M_{\odot}$  (this picture predicts the existence of many Population III stars surviving in the Galaxy till the present day). Given our current poor understanding of the Population III IMF, in this work we choose to work with two different IMFs: 1–100  $M_{\odot}$  Salpeter (“low-mass IMF”) and 100–260  $M_{\odot}$  Salpeter (“high-mass IMF”). The former has metal yields from AGB stars and core-collapse supernovae, while the latter has yields from pair-instability supernovae.

### 3. RESULTS

We now present the results of our model. In Section 3.1, we describe the results of our fiducial model which assumes instantaneous and homogeneous mixing of metals in the ISM, and show that it predicts a very small Population III contribution to reionization. The main reason for this is chemical feedback, which we study in Section 3.2. We then study the conditions under which Population III stars could contribute significantly to reionization, by modelling delayed mixing of metals in the ISM, thereby reducing chemical feedback. In Section 3.3 we look at the constraints from chemical enrichment measurements of high redshift DLAs and argue that these rule out significantly delayed mixing, and hence any significant contribution from high-mass Population III stars.

#### 3.1. Population III Contribution to Reionization

Our model calibration procedure is described in detail in Kulkarni et al. (2013). The model is calibrated by matching (1) the observed cosmic SFR density evolution (Hopkins & Beacom 2006), (2) the fraction of total baryon density in collapsed haloes at  $z = 0$  (Fukugita & Peebles 2004), and the reionization history of the IGM as measured by (3) the electron Thomson scattering optical depth to the last scattering surface (Hinshaw et al. 2012) and (4) the hydrogen photoionization rate evolution (Meiksin & White 2004; Bolton & Haehnelt 2007; Faucher-Giguère et al. 2008; Becker & Bolton 2013).

We assume a constant star-formation efficiency parameter  $f_*$ , defined by

$$\psi = f_* \left( \frac{M_{\text{cool}}}{t_{\text{dyn}}} \right), \quad (1)$$

where  $\psi$  is the halo star formation rate,  $M_{\text{cool}}$  is the cold gas mass in the halo, and  $t_{\text{dyn}}$  is the halo dynamical time. The star-formation efficiency is then tuned to reproduce the cosmic SFR density. For our fiducial model (described below), we have  $f_*$  (Pop. II) = 0.002 and  $f_*$  (Pop. III) = 0.004. Star formation in haloes is accompanied by supernova-induced outflows, the strength of which is fixed by matching the fraction of total baryon density in collapsed haloes at  $z = 0$ .

Once the star formation efficiency is fixed, reionization depends mainly on the escape fraction of ionizing photons,  $f_{\text{esc}}$ , defined as the fraction of ionizing photons that escape the parent galaxy. We assume  $f_{\text{esc}}$  to be independent of redshift and halo mass, and calibrate it to reproduce the observed values of the electron Thomson scattering optical depth,  $\tau_e$  and the hydrogen photoionization rate,  $\Gamma_{\text{HI}}$ . It is crucial to include both these constraints as the observed hydrogen photoionization rate evolution imposes continuity on the epoch of reionization. Our fiducial model has  $f_{\text{esc}} = 0.2$ . Although, in our calibrated model, the IGM electron Thomson scattering optical depth  $\tau_e$  is always obtained in the  $1\sigma$  range of its best-fit value ( $0.089 \pm 0.014$  as given by WMAP9; Hinshaw et al. 2012), our value of  $\tau$  is always closer to the upper-limit of this range. This suggests that an evolving escape fraction is necessary for fitting both  $\tau_e$  and  $\Gamma_{\text{HI}}$  simultaneously (Mitra et al. 2012; Finlator et al. 2012).

We calibrate the model independently for each of the two Population III stellar IMFs considered in this paper. Our fiducial model assumes instantaneous mixing of metals in the ISM. We describe the results of this model in this section. We discuss the effect of relaxing the instantaneous mixing assumption in subsequent sections.

### 3.1.1. Population III SFR

Fig. 1 shows the results of our fiducial model. Panel (c2) shows the predicted total (Population II + Population III) cosmic SFR density evolution for the two different Population III IMFs (low-mass IMF in black and high-mass IMF in red). The red data points are observational measurements from a compilation by Hopkins & Beacom (2006), in which consistent dust obscuration corrections, SFR calibrations, and IMF assumptions are applied to ultraviolet and far-infrared data. Our model predictions are in good agreement with the data regardless of what Population III IMF is assumed. Indeed, the total SFR density in the two cases is nearly identical (the red and black solid curves overlap), because the contribution of Population III star formation to the total SFR is very low over most of the cosmic history. The Population III SFR density evolution is shown separately by the dashed curves. The corresponding panel (c1) shows the fraction of the total SFR produced by Population III star formation. We find that the contribution of Population III stars to the total SFR density is low (less than 10%) throughout most of the age of the Universe. It is greater than 10% for less than 100 Myr ( $z > 40$ ). Population III stars dominate the cosmic

SFR density for an even smaller time period at  $z \sim 50$  (cf. Naoz et al. 2006). By the time that galaxies are observable at  $z < 8$ , all haloes capable of forming stars (i.e., above the minimum mass for star-formation) have already enriched themselves above the critical metallicity, and hence the Population III SFR is zero at these late times. Thus, although Population III stars initiate the epoch of reionization, they quickly relinquish their dominant role by enriching their environment. We discuss the reason behind this below.

We note that the star formation history shown in Fig. 1, together with our chemical evolution model, is also consistent with the observed mass-metallicity relations (Erb et al. 2006; Maiolino et al. 2008) at redshifts 2.3 and 3.7 (see Kulkarni et al. 2013 for details). The corresponding IGM metallicity is also consistent with observational estimates (Schaye et al. 2003; Simcoe et al. 2004). We also note here that the difference between the two Population III SFR density curves (dashed curves) in panel (c2) of Fig. 1 can be understood from the different metal yields for the two Population III IMFs (recall that the Population II IMF is the same in both cases). The high-mass IMF has a larger metal yield. As a result, in this case haloes are enriched beyond  $Z_{\text{crit}}$  earlier as compared to the low-mass IMF, and Population III star formation is terminated earlier. This is reflected in the reduced level of Population III SFR density for the high-mass IMF.

### 3.1.2. Photoionization rate

The small contribution of Population III stars to the total cosmic SFR density suggests that their contribution to reionization will also be small. This is seen in panel (b2) of Fig. 1, which shows the evolution of the hydrogen photoionization rate in our model. Making the so-called local source approximation, which is valid for spectral indices typical to star-forming galaxies, the hydrogen photoionization rate is given by

$$\Gamma_{\text{HI}}(z) = (1+z)^3 \int_{\nu_{912}}^{\infty} d\nu \lambda(z, \nu) \dot{n}_\nu(z) \sigma(\nu), \quad (2)$$

where  $\sigma(\nu)$  is the photoionization cross-section of hydrogen,  $\lambda(z, \nu)$  is the redshift-dependent mean free path of ionizing photons. We calculate the mean free path of ionizing photons as in Paper 1 by integrating over the lognormal density PDF of the IGM and estimating the average distance between high-density, neutral regions. This method is calibrated to reproduce the incidence rate of Lyman-limit systems at low redshifts (Miralda-Escudé et al. 2000; Choudhury & Ferrara 2005; Prochaska et al. 2009). Our model agrees with the measurement of Prochaska et al. (2009). The quantity  $\dot{n}_\nu(z)$  is the number density of ionizing photons in the IGM per unit time, and is given by

$$\dot{n}_\nu(z) = f_{\text{esc}} \dot{\rho}_*(z) \int dm \phi(m) t_{\text{age}}(m) Q_H(m). \quad (3)$$

The integral in this equation is over stellar masses and takes the IMF-dependence of the ionizing photon flux into account:  $\phi(m)$  is the normalised stellar IMF,  $t_{\text{age}}(m)$  is the age of a star with mass  $m$  and  $Q_H(m)$  the stellar hydrogen-ionizing photon flux (in photons  $\text{s}^{-1}$ ) provided

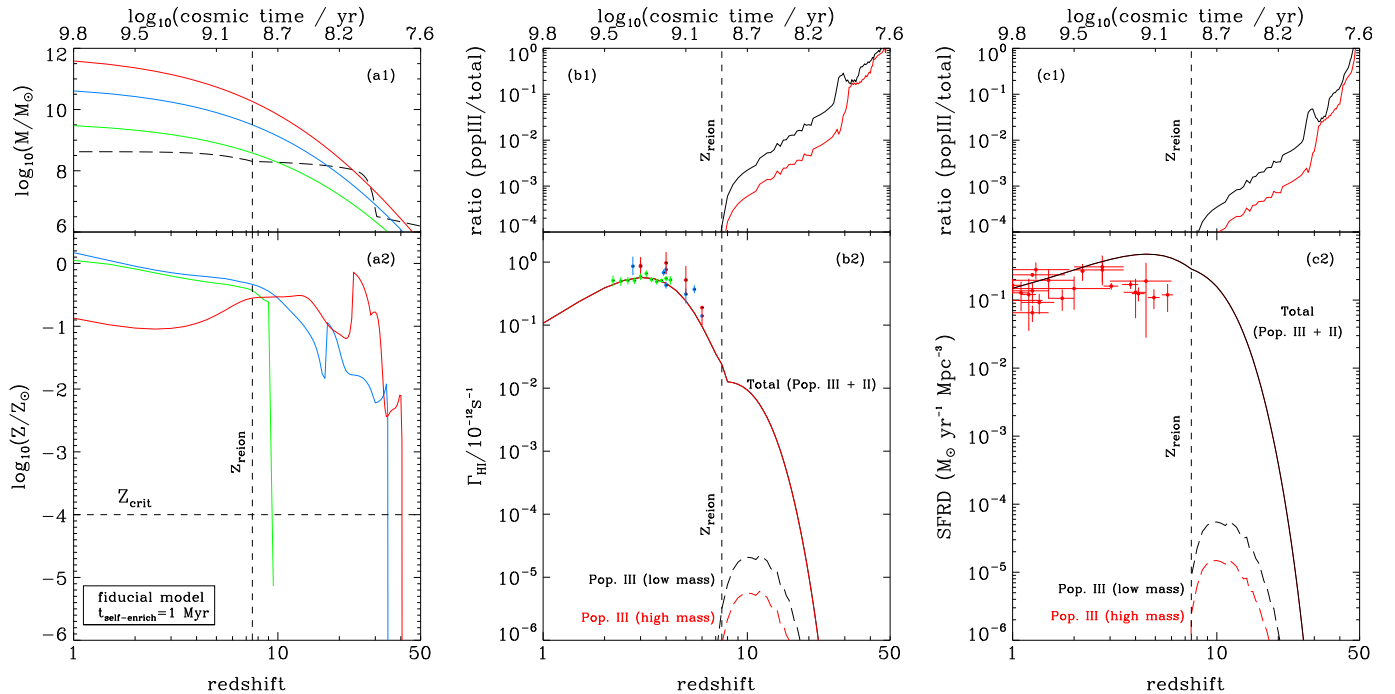


**Figure 1.** Results for our fiducial model. Panels (a1) and (a2) show the metallicity evolution for three particular halo masses for illustration. The long-dashed curve in panel (a1) shows the evolution of  $M_{\min}$  in cosmological H II regions. Panel (b1) and (b2) show the evolution of the hydrogen photoionization rate and the contribution to it from Population III stars for the two models considered. The corresponding panel (b1) plots the ratio of the two quantities. In this panel, the black curve corresponds to the low-mass IMF model and the red curve to the high-mass IMF model. Panels (c1) and (c2) show the evolution of the cosmic SFR density in the model and the contribution from Population III stars. Vertical dashed lines in all panels show the redshift of reionization.

by stellar evolution models (Schaerer 2002). The quantity  $f_{\text{esc}}$  is the escape fraction of ionizing photons that accounts for the fraction of the ionizing photons that escape into the IGM. The escape fraction is a free parameter of our model. In this paper, we assume that  $f_{\text{esc}}$  is constant at all redshifts. We comment on the effect of this assumption below. Our fiducial model has  $f_{\text{esc}} = 0.2$

In panel (b2) of Fig. 1, the data points are measurements of the hydrogen photoionization rate as deduced from the mean opacity of the hydrogen Ly $\alpha$  forest (Meiksin & White 2004; Bolton & Haehnelt 2007; Faucher-Giguère et al. 2008), where we note that there is disagreement between the measurements at the factor-of-two level, which likely results from different assumptions about the density distribution and thermal state of the IGM. Here we choose to fit the data by Faucher-Giguère et al. (2008) but this choice is not critically important for our main result. The solid curves in panel (b2) of Fig. 1 show the model predictions corresponding to two different Population III IMFs (low-mass IMF in black and high-mass IMF in red). The model predictions agree very well with the observational measurements.<sup>4</sup> As seen by the evolution of the hydrogen photoionization rate, reionization in our model is gradual. It begins at  $z \gtrsim 30$  and is 90% complete by  $z \sim 7$ . This gradual change in the ionization state of the IGM helps us simultaneously reproduce the observed electron scattering optical depth  $\tau_e = 0.089 \pm 0.014$  (Hinshaw et al.

2012) and the photoionization rate data. Before reionization at  $z_{\text{reion}} = 7.5$ , the photoionization rate increases rapidly as UV photon sources build up. There is a sudden jump at  $z = z_{\text{reion}}$  when different H II regions overlap. (This redshift is marked by the vertical dashed line in Fig. 1). This is because at this redshift, a given point in the IGM starts “seeing” multiple sources, which rapidly enhances the UV photon mean free path, thereby affecting the photoionization rate. Secondly, Fig. 1 also shows that the contribution of Population III stars to reionization is small. This is clear from the overlap between the red and black solid curves in panel (b2), and is evident in the dashed curves, which show the contribution to  $\Gamma_{\text{HI}}$  by Population III stars. We see that the Population III contribution to photoionization rate is subdominant over most of the reionization history. Panel (b1) of Fig. 1 further highlights this by showing the fraction of the H I photoionization rate contributed by Population III star-formation, relative to the total rate. Except at the earliest stages of galaxy formation ( $z \sim 50$ ), the ratio is much less than unity. For the low-mass IMF, the ratio is less than 10% for  $z \lesssim 20$ , and for the high-mass IMF, it is less than 10% for  $z \lesssim 30$ .

### 3.1.3. Understanding the Low Population III Contribution

We now discuss the reason behind the small contribution of Population III stars to reionization in our model. This contribution depends on three parameters of the model: (1) the efficiency with which cold gas is converted into stars, (2) the escape fraction of ionizing radiation, and (3) chemical feedback, quantified by the time scale over which a halo enriches itself beyond the critical metallicity  $Z_{\text{crit}}$  and stops the formation of Popula-

<sup>4</sup> Note that we have ignored the ionizing photon contribution from quasars in our model, which are expected to only contribute significantly for  $z < 3$  (Fontanot et al. 2012) and we do not expect any Population III contribution at these late times.

tion III stars. These three factors are not independent of each other: a higher efficiency of star formation reduces the self-enrichment time scale of a halo, and a higher  $f_{\text{esc}}$  requires us to reduce the star formation efficiency if we are to satisfy the observational constraints on reionization. In our model, the constraints from  $\Gamma_{\text{HI}}$ ,  $\tau_e$  and the cosmic SFR density completely fix the star formation efficiency and the escape fraction. Therefore, as we assume instantaneous metal mixing in our fiducial model, the self-enrichment time scale is also fixed.

Panel (a2) of Fig. 1 shows the metallicity evolution of three different haloes in our model, which helps one understand the small contribution of Population III stars to reionization in our model (for simplicity, we show results only for the high-mass IMF in this panel, but the low-mass IMF gives similar trajectories). The horizontal dashed line in this panel shows the critical metallicity  $Z_{\text{crit}}$ , which we always take to be  $10^{-4}Z_{\odot}$ . The mass assembly history of these haloes is shown in the corresponding panel (a1); their masses at  $z = 0$  are about  $10^{10} M_{\odot}$ ,  $10^{11} M_{\odot}$ , and  $10^{12} M_{\odot}$  respectively. The dashed curve in the panel (a1) shows the evolution of the minimum mass of star-forming haloes,  $M_{\text{min}}$ , which is set according to the Jeans criterion, which in turn depends on the thermal evolution of the IGM (see, e.g., Rorai et al. 2013, for a recent discussion). To be specific, here we consider haloes that collapse in cosmological H II regions, and the  $M_{\text{min}}$  evolution shown corresponds only to these regions (but the discussion could be easily generalized to H I regions). In these regions,  $M_{\text{min}}$  is roughly constant at  $\sim 10^8 M_{\odot}$  as this evolution is only determined by the Jeans scale corresponding to the characteristic temperature of the IGM at  $T \sim 10^4$  K. In each halo’s assembly history, star formation begins when its mass crosses the threshold set by  $M_{\text{min}}$ . This is manifest in the metallicity evolution history of each halo as shown in panel (a2). It is seen that the halo metallicities increase mostly monotonically.<sup>5</sup> Additionally, in each case, the initial burst of Population III stars is sufficient to rapidly enhance the ISM metallicity beyond  $Z_{\text{crit}}$ . This metallicity evolution is in good agreement with the hydrodynamic simulations of Wise et al. (2012). It is exactly this prompt enrichment of the ISM of high-redshift galaxies which causes an early cut-off in the Population III SFR. The range of redshifts in panel (c2) that show sub-dominant Population III SFR, arises from only the lowest mass star-forming halos, which only recently crossed the minimum mass threshold. However, the vast majority of star-forming halos at higher masses have already been chemically self-enriched by this time, and have stopped forming Population III stars, which in turn reduces the overall contribution of Population III stars to the photoionization rate. As previously mentioned above, apart from the star formation efficiency assumed in the model, the rapid enrichment of galaxies is a result of the assumption that metals are instantaneously mixed in the ISM gas. We discuss the assumption in detail in the next section.

Finally, we briefly note that haloes down to a mass limit of  $M_{\text{min}} \sim 10^8 M_{\odot}$  contribute to the ionization

<sup>5</sup> Some non-monotonicity seen in panel (a2) of Fig. 1 is due to the behaviour of  $M_{\text{min}}$  at the highest redshift, which can restrict gas inflow into haloes at certain times, affecting the metallicity.

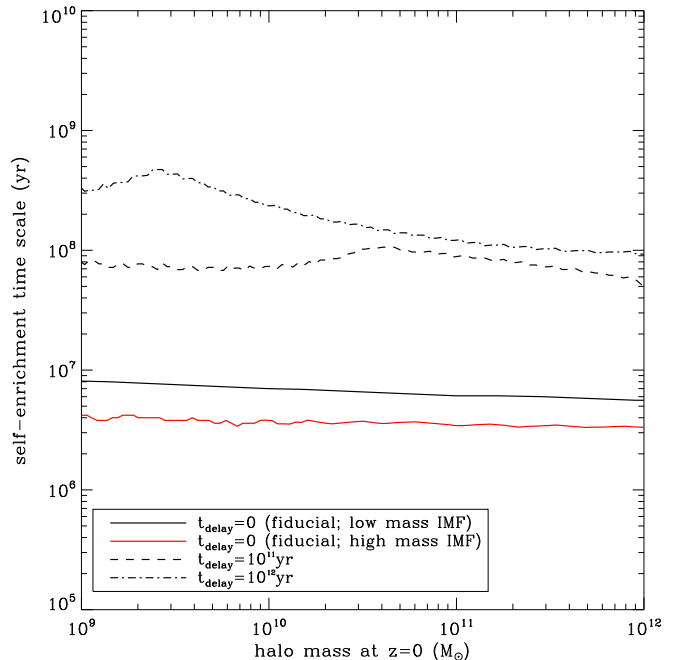


**Figure 2.** Halo self-enrichment time scale in our model, defined as the time between the first star-formation episode of the halo and the time at which its gas-phase metallicity crosses  $Z_{\text{crit}}$ . It quantifies the time scale of Population III star formation in a given halo. Halo mass at  $z = 0$  serves as a label for different haloes. The solid curves show the time scale for the fiducial models. Other curves show the time scale for models with delayed enrichment.

flux in Eqn. (3). At  $z \sim 7$  this corresponds to a UV magnitude to  $M_{1500} = -10$  in our model, which agrees well with the very faint minimum galaxy magnitude, to which the UV luminosity function of Lyman break galaxies (LBGs) must be extrapolated in order to reionize the universe (Kuhlen & Faucher-Giguère 2012; Fontanot et al. 2012; Robertson et al. 2013). Furthermore, the halo masses which we deduce for these faint galaxies  $M_{\text{min}} \sim 10^8 M_{\odot}$  agree well with masses deduced using abundance matching (Trenti et al. 2010; Kuhlen & Faucher-Giguère 2012). This indicates that in our fiducial model, it is the faint galaxies that produce the bulk of the ionizing photons that reionized the IGM, and not Population III stars.

### 3.2. The Halo Self-Enrichment Timescale

In the results presented above, metals injected into the ISM by supernova explosions are assumed to be instantaneously mixed into the halo ISM. Instantaneous and homogeneous mixing of metals is a standard assumption in galactic chemical evolution studies (Tinsley 1980; Pagel 2009; Matteucci 2012) and is responsible for the early termination of Population III star formation in our fiducial model. Note that we are not assuming instantaneous recycling, since we directly model the delay in the synthesis of new metals due to finite stellar lifetimes. However, we have assumed instantaneous mixing, which is to say that after a supernova event, newly liberated metals are instantaneously available in the ISM to influence the next generation of star-formation. We have seen in our fiducial model, that the initial burst of Population III stars is sufficient to enhance the ISM metallicity beyond  $Z_{\text{crit}}$  in any halo mass bin over a very short time scale. When this

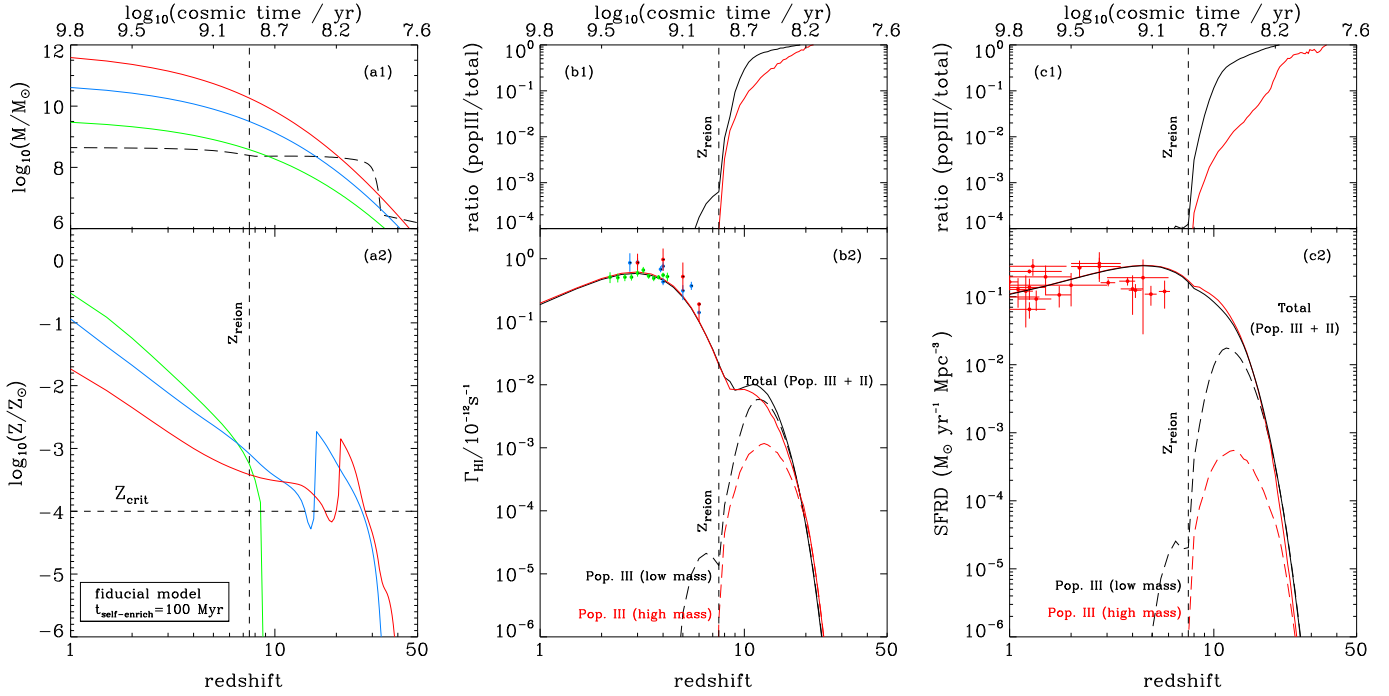


**Figure 3.** Same as Fig. 1 but for a model in which metal enrichment in ISM is gradual with a delay time of  $t_{\text{delay}} = 10^{11}$  yr. This increases the self-enrichment time scale of haloes to about  $10^8$  yr. Consequently, the contribution of Population III stars to the cosmic star formation rate and to the hydrogen photoionization rate is enhanced relative to the fiducial model. See text for details.

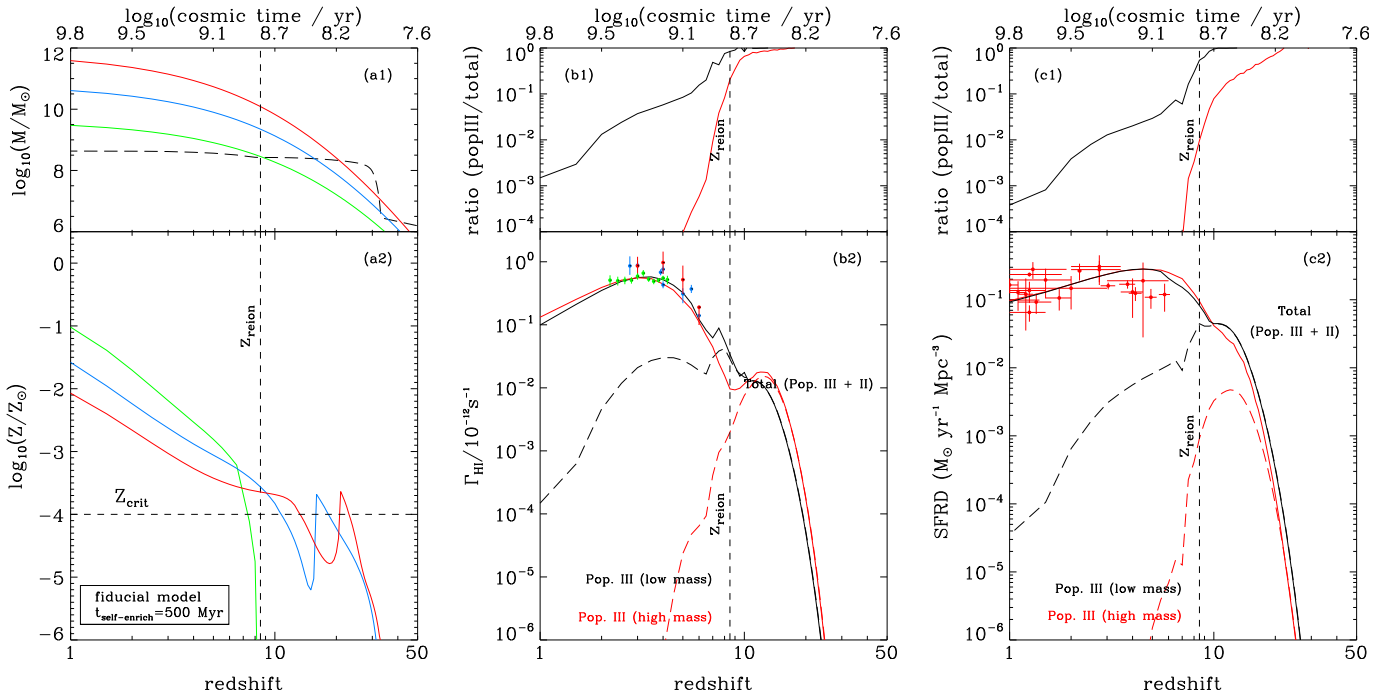


**Figure 4.** Same as Figs. 1 and 3 and but for a model in which metal enrichment in ISM is gradual with a delay time of  $t_{\text{delay}} = 10^{12}$  yr, i.e., an order-of-magnitude slower than in Fig. 3. This further increases the self-enrichment time scale of haloes to about  $4 \times 10^8$  yr. As a result, the contribution of Population III stars to the cosmic star formation rate and to the hydrogen photoionization rate is high enough to complete hydrogen reionization. Note that in this model, the redshift of reionization is slightly different for the two Population III IMFs; we only show the low-mass IMF case for simplicity.

happens, the corresponding galaxy stops forming Population III stars. Since most of the mass in the universe is contained in  $M_*$  haloes, the Population III cosmic SFR density begins to decline as soon as these haloes cross the  $Z_{\text{crit}}$  threshold. This is the crucial effect that reduces the contribution of Population III stars, and that was not captured in previous models because they did not track chemical enrichment for a large population of haloes in a cosmological volume. We now discuss the dependence of this result on our assumption of instantaneous mixing.

The solid lines in Fig. 2 show the self-enrichment time scale as a function of halo mass for the two Population III IMFs in our fiducial model, where the low-mass IMF is shown in black and high-mass IMF in red. We define the self-enrichment time scale as the time between the first star-formation episode of the halo and the time at which its gas-phase metallicity crosses  $Z_{\text{crit}}$ . In this plot, haloes are labelled by their mass at  $z = 0$ ; their actual mass value at the time of crossing  $M_{\text{min}}$  is not shown. In the low-mass IMF case (solid black), the time scale is a few times  $10^6$  yr. Pair-instability SNe have higher metal output, which results in a shorter enrichment time scale by a factor of 3 in the high-mass IMF case (solid gray). As discussed in section 3.1, it is this short self-enrichment time scale that restricts the contribution of Population III stars to reionization. Note that these curves have a very flat dependence on halo mass because the self-enrichment time scale depends primarily on stellar lifetimes.

In the ISM of a galaxy, mixing of metals ejected by supernovae is carried out by different mechanisms on different length scales: diffusive dispersion due to large-scale motion on kpc scales, turbulent diffusion on pc scales, and molecular diffusion on smaller scales. As a result, the self-enrichment time scale is decided by (1) the respective time scales of these mixing processes, (2) the rate of metal production by supernovae, and (3) rate of interaction with the environment, via inflows and outflows of gas. In our fiducial model, the time scale of the mixing processes is assumed to be zero and therefore the self-enrichment time scale depends only on the stellar lifetimes via the supernova rate. This is the reason behind the short self-enrichment time scale shown in Fig. 2. We now relax this instantaneous mixing assumption.

Supernova-driven metal-mixing in the interstellar medium has been studied using hydrodynamical simulations by de Avillez & Mac Low (2002), who used tracer particles in a simulation of a  $1 \times 1 \times 20$  kpc<sup>3</sup> region of the Galactic disk and found mixing time scales between  $10^6$  and  $10^8$  yr (see their Fig. 8) for supernova rates of  $\sim 1$  to  $\sim 100$  times the Galactic supernova rate. The lower end of this range is of the same order of magnitude as the self-enrichment time scale in our fiducial model. But the results of these simulations suggest that the mixing time scale could very well be two or three orders of magnitude larger.

We consider the effect of longer self-enrichment time scales on our result by implementing a “mixing function”,  $f(t)$ , which governs the rate at which metals are mixed in the ISM. The source term due to star formation in the metallicity evolution equation is of the form (Eqn. 19 in

Kulkarni et al. 2013)

$$\dot{M}_Z(z) = \int_{m_l}^{m_u} dm \phi(m) \cdot \psi[t(z) - \tau(m)] \times mp_Z(m), \quad (4)$$

where  $m$  is the stellar mass,  $\psi(t)$  is the star formation rate at time  $t$ ,  $\phi(m)$  is the stellar IMF,  $\tau(m)$  is the stellar age, and  $p_Z(m)$  is the mass fraction of a star of initial mass  $m$  that is converted to metals and ejected. The limits  $m_l$  and  $m_u$  define the range of stellar masses considered in the IMF. To relax the instantaneous mixing assumption, we modify Eqn. (4) to

$$\dot{M}_Z(z) = \int_{m_l}^{m_u} dm \phi(m) mp_Z(m) \times \int_{t(z)-t_{\text{delay}}}^{t(z)} d\tilde{t} \psi[\tilde{t}(z) - \tau(m)] f(\tilde{t}), \quad (5)$$

where  $f(\tilde{t})$  is a mixing function that serves to delay the mixing of metals in the ISM after a supernova event. The mixing function is defined over a time duration of  $t_{\text{delay}}$ . In this picture, after a supernova has exploded, the resulting metal mass is added to the ISM gradually over a time  $t_{\text{delay}}$ . Until this time, we imagine the metals to be locked up into un-mixed pockets of the ISM, and so they are not available for future star-formation. Thus, our fiducial model corresponds to the case where the mixing function is a delta function with  $t_{\text{delay}} = 0$  yr. For non-zero values of  $t_{\text{delay}}$ , the ISM metallicity can remain below the critical metallicity  $Z_{\text{crit}}$  for a longer time compared to our fiducial model. Therefore, we would expect that in this case, Population III star formation will continue for a longer period, and possibly impact reionization. The mixing function is determined by the complex interplay of various mixing processes in the ISM. The most conservative form of the mixing function is a constant of the form

$$f(t) = \begin{cases} t_{\text{delay}}^{-1} & \text{if } t < t_{\text{delay}} \\ 0 & \text{otherwise,} \end{cases} \quad (6)$$

where  $t$  is the time since a supernova explosion.<sup>6</sup> Note that  $f(t)$  is normalised such that all of the supernova ejecta is mixed in the ISM over the period  $t_{\text{delay}}$ . We adopt this simple form for the mixing function in this paper. Figs. 3 and 4 show the results of our model with this mixing function and  $t_{\text{delay}} = 10^{11}$  yr and  $t_{\text{delay}} = 10^{12}$  yr respectively. The self-enrichment time scales in these models is compared to that in our fiducial model in Fig. 2 (only the high-mass Population III IMF case is shown for simplicity). Given that we have adopted a mixing timescale which is much longer than the age of the Universe, i.e.,  $t_{\text{delay}} = 10^{10}$  or  $10^{11}$  yr, the effective result is that at  $z \sim 10$ , where  $t_{z=10} \sim 10^9$  yr, these mixing models imply that only 1% and 0.1% of the metals produced by Population III SNe are mixed into the ISM, respectively. As we will see below even this small amount

<sup>6</sup> This form of the mixing function is the most conservative in the sense that all time instances from 0 to  $t_{\text{delay}}$  are treated equally. As a result, metals are mixed into the ISM at a constant rate and, in the limit of an exactly closed system, the metallicity would increase linearly.

of metals is still enough to produce significant chemical feedback that influences Population III star formation. This results because as shown in panel (a2) of Fig. 1, a single generation of Population III SNe injects enough metals to raise the the ISM metallicity of  $M_*$  halos to a  $Z \sim 10^{-1}Z_\odot$  by  $z \sim 10$ , if these metals are instantaneously mixed. Thus reducing this yield by a factor of  $\sim t_{z=10}/t_{\text{delay}} \sim 100$ , as in the case when  $t_{\text{delay}} = 10^{11}$ , is still sufficient to be in excess of the critical metallicity. For this reason, and as is also clear from the mathematical form of Eqn. 5, we generally expect a non-linear dependence of the self-enrichment timescale on  $t_{\text{delay}}$ , and similarly the dependence of Population III star-formation on  $t_{\text{delay}}$  will also be nonlinear. For instance, between Fig. 3 and Fig. 4, changing  $t_{\text{delay}}$  by a factor of 10 results in small changes of factor of 3 in the self-enrichment time scale.

In Fig. 3 the same curves illustrating the star-formation, reionization, and enrichment history as in Fig. 1 are shown but for a model with  $t_{\text{delay}} = 10^{11}$  yr. As expected, and illustrated in panel (a2) of Fig. 3, haloes now take longer to cross the  $Z_{\text{crit}}$  metallicity threshold, compared to the fiducial model (panel a2 of Fig. 1, which is on the same scale). This increases the cosmic Population III SFR density, which, although still subdominant, contributes more than 10% of the total SFR density at redshifts above  $z \sim 20$  in the high-mass Population III IMF run (the corresponding redshift value for the fiducial model was  $z \sim 30$ ). The relative increase in Population III star-formation also manifests as an increase in the hydrogen photoionization rate, which is also enhanced relative to the fiducial model. Indeed, the contribution of Population III stars to the hydrogen photoionization rate at  $z = 10$  is 10% for the high-mass case, whereas the contribution was less than 1% at this redshift in our fiducial model. Thus for  $t_{\text{delay}} = 10^{11}$  yr, the contribution of Population III stars to reionization is subdominant but significant. Note that these numbers are slightly different for the low-mass case for the same mixing function and  $t_{\text{delay}}$ . In general, low mass Population III star formation lasts longer than for the high-mass IMF. This is because the metal yields of high mass Population III stars is higher than those of low mass stars, resulting in larger chemical feedback, and earlier termination of Population III.

Fig 4 shows the results of the model with  $t_{\text{delay}} = 10^{12}$  yr, for which the mixing of metal metals is even more gradual. The impact of Population III on cosmic star-formation and the ionizing photon budget is now increased in magnitude relative to the previous case shown in Fig. 3. For instance, all star formation for  $z \gtrsim 10$  in this model is Population III, regardless of the Population III IMF. Thus the process of hydrogen reionization is almost single-handedly carried out by Population III stars. The contribution of Population III stars to the hydrogen photoionization rate at  $z = 10$  is about 60% for the high-mass case, and 100% for the low-mass case. Their contribution to the cosmic SFR density at  $z = 10$  is about 20% for the high-mass case, and 80% for the low-mass case. Similar to the results in Fig. 3, the Population III contribution is higher for low-mass Population III IMF because of weaker chemical feedback.

Fig. 2 helps in visualising the effect of the mixing function on our model. The self-enrichment time scale in the

two variant models is longer than that in the fiducial model by more than an order of magnitude. The increase, however, is still less than  $t_{\text{delay}}$ , as only a fraction of metals are required to increase halo metallicity beyond  $Z_{\text{crit}}$ .

A general lesson from above is that due to constraints imposed by the measurements of cosmic SFR density, the hydrogen photoionization rate, and the electron scattering optical depth, the contribution of Population III stars to reionization can be enhanced only by increasing the metal mixing time scale assumed in the model. This contribution is generally predicted to be small unless the self-enrichment time scale is  $\gtrsim 3 \times 10^8$  yr.

### 3.3. Chemical Enrichment Constraints on the Contribution of Population III to Reionization

By varying the assumptions about the Population III IMF and the metal mixing timescale, we have seen that the self-enrichment timescale can take on values between  $3 \times 10^6$ – $3 \times 10^8$  years, dramatically impacting the chemical feedback which eventually terminates Population III star formation. These degrees of freedom result in concomitant uncertainties on the contribution of Population III star-formation to the ionizing photon budget of 1–100%, since all of the models were able to match the star-formation and reionization observables that we considered. However, we can discriminate between these possibilities using accurate chemical enrichment observations in damped Ly $\alpha$  absorbers (DLAs) at post-reionization redshifts. Observations of DLAs can be used to measure gas-phase metallicities at large cosmological lookback times with high precision. Furthermore, relative abundances can still be measured accurately deep into the reionization epoch ( $z > 6$ ) using metal-line transitions redward of Ly $\alpha$ , even though Gunn-Peterson absorption precludes measurement of neutral hydrogen. In Kulkarni et al. (2013) we modeled the chemical evolution of DLAs, and showed how their abundance patterns can be used to constrain Population III scenarios. Here we argue that they can also constrain the contribution of Population III stars to reionization.

In our model, we assigned a mass-dependent H I absorption cross-section, denoted by  $\Sigma$  to each halo in order to predict the expected distribution of DLA abundance ratios (see Kulkarni et al. 2013 for details). This assignment is motivated by hydrodynamical simulations (Gardner et al. 1997, 2001; Nagamine et al. 2004a,b, 2007; Pontzen et al. 2008) and reproduces the observed DLA metallicity evolution (Rafelski et al. 2012), incidence rate (Prochaska et al. 2005; Noterdaeme et al. 2012), and clustering bias (Font-Ribera et al. 2012) at low redshifts ( $z \sim 3$ ) very well, and takes the form

$$\Sigma(M) = \Sigma_0 \left( \frac{M}{M_0} \right)^2 \left( 1 + \frac{M}{M_0} \right)^{\alpha-2}, \quad (7)$$

where the constants take the values of  $\alpha = 0.2$ ,  $M_0 = 10^{9.5} M_\odot$ , and  $\Sigma_0 = 40 \text{ kpc}^2$  at  $z = 3$  (Pontzen et al. 2008; Font-Ribera et al. 2012). Values at other redshifts are calculated by mapping haloes at these redshifts to haloes  $z = 3$  according to circular velocity (Font-Ribera et al. 2012). With this assignment, for any measurable property  $p$  (e.g., abundance ratio  $[M_1/M_2]$ ) of DLAs, we can calculate the number of systems with

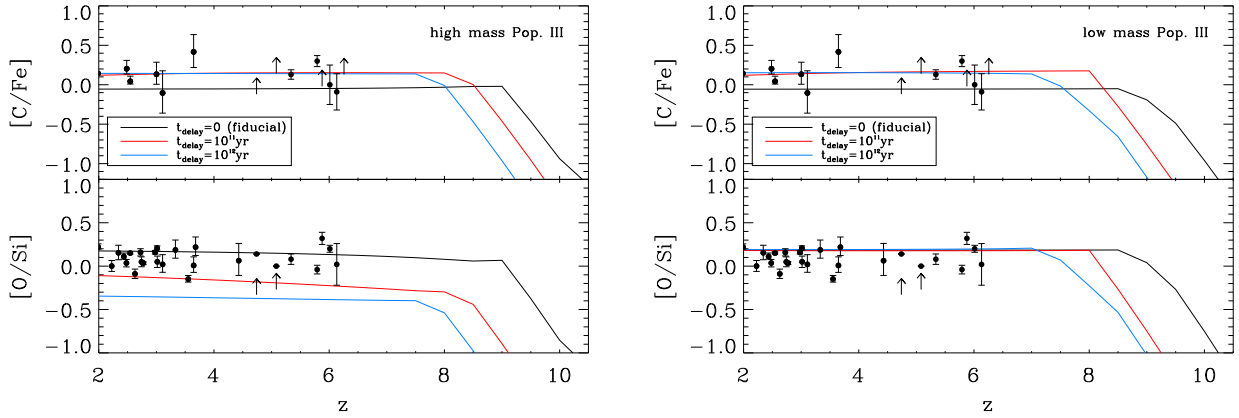


**Figure 5.** Evolution of mean values of  $[C/Fe]$  and  $[O/Si]$  DLA relative abundances in all models considered in this paper. Data points show observed DLA relative abundances from a compilation by [Becker et al. \(2012\)](#). Right panel shows low-mass IMF models, left panel high-mass IMF models. Our fiducial model (black curves) is consistent with the observational measurements. The high-mass IMF model with gradual enrichment with  $t_{\text{delay}} = 10^{11}$  yr is only marginally consistent with the  $[O/Si]$  data, while that with  $t_{\text{delay}} = 10^{12}$  yr is ruled out by the data. This constrains the Population III contribution to reionization. Note that the low-mass IMF models are harder to rule out, as discussed in the text.

different values of  $p$  in a sample of DLAs. This is called the line density distribution, and with Eqn. (7) in hand, it can be written as (e.g., [Wolfe et al. 2005](#))

$$\frac{d^2 N}{dX dp} = N(M) \cdot \Sigma(M) \cdot \frac{dl}{dX} \frac{dM}{dp} \cdot (1+z)^3. \quad (8)$$

Here,  $X$  is an absorption length element given by

$$\frac{dl}{dX} = \frac{c}{H_0(1+z)^3}, \quad (9)$$

$dl = cdt$  is a length element, and  $p$  is the property in consideration. The halo mass is denoted by  $M$ ,  $N(M)$  is the comoving number density of halos (i.e., the halo mass function), and  $\Sigma(M)$  is the halo cross section given by Eqn. (7). The quantity  $dM/dp$  in Eqn. (8) can be easily calculated in our model, as properties like metallicity and relative abundances are known for all halo masses. The integral of Eqn. (8) over all values of  $p$  is just the total line density of DLAs,  $dN/dX$ . The average value of  $p$  in an observed sample of DLAs is given by

$$\langle p \rangle = \int \frac{d^2 N}{dX dp} \cdot p \cdot dp \cdot dX. \quad (10)$$

Fig. 5 shows the result of evaluating Eqn. (10) for  $p = [C/Fe]$  and  $[O/Si]$  in our fiducial model and its variants. It also shows the observed evolution of  $[C/Fe]$  and  $[O/Si]$  relative abundances in DLAs. The  $z \sim 2-4$  measurements are from [Dessauges-Zavadsky et al. \(2003\)](#); [Péroux et al. \(2007\)](#); [Cooke et al. \(2011\)](#) and  $z > 4$  measurements are from [Becker et al. \(2012\)](#), as compiled by [Becker et al. \(2012\)](#). Over a time period of about 6 Gyr (from  $z = 2$  to  $z = 6$ ), these abundance ratios are relatively constant. Furthermore, they show little scatter around the mean. Solid lines in Fig. 5 show the evolution of these relative abundances in our low-mass IMF models, while the dashed lines show the evolution in the high-mass IMF case. Curves with different colors indicate different delay times.

Our fiducial model agrees with data for both  $[C/Fe]$  as well as  $[O/Si]$ . In this redshift range, the mean values of these abundance ratios in this model are governed by the Population II IMF as the contribution of Popula-

tion III stars is erased in all but the smallest haloes. The asymptotic value of these abundance ratios towards low redshift thus simply reflects the relative yields of these elements per star integrated over the Population II IMF.

However, the variants of the fiducial model, in which Population III contribution to the cosmic SFR and photoionization rate is higher, disagree with current relative abundance measurements. We first discuss the high-mass IMF models. As described in the previous section, we considered two variants where metals are gradually mixed in the ISM over a period of  $t_{\text{delay}} = 10^{11}$  yr and  $10^{12}$  yr respectively, resulting in corresponding self-enrichment time scales of  $10^8$  and  $5 \times 10^8$  yr. As shown in Figs. 3 and 4, the first of these models has more than 20% Population III contribution to the photoionization rate down to  $z \sim 20$ , while in the second model the contribution is more than 20% all way down to  $z \sim 10$ . We now see in Fig. 5 that the model with  $t_{\text{delay}} = 10^{11}$  yr is marginally ruled out by the existing  $[O/Si]$  data (red dashed curve in bottom panel of Fig. 5), while the model with  $t_{\text{delay}} = 10^{12}$  yr is completely ruled out. In the previous section we showed that the contribution of Population III stars to reionization could only be enhanced by increasing the metal-mixing time scale, however this results in a corresponding increase in the chemical vestiges of these Population III stars. Fig. 5 shows that the DLA relative abundance measurements actually restrict the high-mass Population III contribution to reionization to be less than 10% for  $z \lesssim 15$ . The model with  $t_{\text{delay}} = 10^{11}$  yr acts as a kind of upper bound on the self-enrichment time scale of haloes and therefore on the role that high-mass Population III stars play in hydrogen reionization. The  $[O/Si]$  ratio is more constraining than  $[C/Fe]$  because of significant variation in the Si yield with IMF: the high-mass IMF produces two orders of magnitude higher Si yield as Si is efficiently produced in massive stars due to O-burning.

The contribution of low-mass Population III stars to reionization is harder to constrain using DLA chemical data. This is because chemical yields of low-mass Population III stars are not very different from those of Population II stars considered in our models, as the two IMFs have similar shapes and mass ranges. (There is some

difference in the yields due to difference in their metallicities.) Thus we see in Fig. 5 that the [O/Si] values in all our low-mass IMF models are consistent with the data, regardless of mixing delay and self-enrichment timescale. This is also true for the [C/Fe] abundance ratio, although the values are slightly different from the fiducial case, because the yields are different and the large mixing time scale slows dilution by Population II yields. However, even if we cannot rule out the low-mass IMF case, it is worth noting that the ionizing emissivity of low mass Population III stars is only a factor of two higher than that of Population II stars. Therefore reionization by these stars is qualitatively similar to reionization by Population II stars alone.

Finally, we note that the exact behaviour of the curves in Fig. 5 depends on the form of the mixing function used. A mixing function different from that in Eqn. 6 will in general result in a different evolution of the mean relative abundances. However, the primary result of Fig. 5 is more general: any Population III star formation activity that produces hydrogen-ionizing photons at these redshifts will also necessarily produce Population III chemical signatures, which can be constrained using measurements of abundance patterns in DLAs. Also DLA relative abundance measurements at  $z \sim 8$ , using background QSOs or GRBs, could start to constrain even the low-mass Population III IMF by witnessing the build-up of the metallicity in halos and change in relative abundances with time because of finite stellar lifetimes.

#### 4. CONCLUSION

In this paper, we have demonstrated that Population III stars contribute very little to the cosmic SFR density and to the reionization history. This is because the halos dominating the cosmic star-formation rate at high-redshift rapidly (time scales of only  $\sim 10^7$  yr) self-enrich to the critical metallicity, terminating Population III star formation. We quantify this rapid self-enrichment by defining a halo self-enrichment time scale, which is  $\sim 10^6$  yr in our fiducial model. This time scale is set by stellar lifetimes, and is almost independent of halo mass. Although this rapid self-enrichment occurs at different redshift in halos of different masses, the net effect is to reduce the Population III star formation and contribution to the hydrogen photoionization rate to less than 1% of the total at  $z = 10$  in our fiducial model.

Previous studies did not uncover this rapid chemical feedback of Population III star-formation, because they did not implement a self-consistent chemical enrichment model, as we have done here. Since our fiducial model assumes instantaneous mixing of metals in the ISM, we studied how relaxing this assumption impacts our results. By slowing the rate at which metals mix into the ISM, we found that the termination of Population III star-formation can be delayed, thus increasing their contribution to reionization. However, mixing delay times and the resulting self-enrichment timescales cannot be arbitrarily long. This is because relative metal abundance patterns in DLAs retain the chemical signatures of Population III SNe, thus providing a chemical record of the Population III star-formation history. Indeed, we find that halo self-enrichment timescales significantly longer than  $10^8$  yr produce abundance patterns that are significantly different from those observed in DLAs at  $z \lesssim 6$ ,

and are thus ruled out. As a result, the maximum allowed delay time implied by existing observations restricts the fractional contribution of high-mass Population III stars to the ionization rate to be  $\lesssim 10\%$  at  $z = 10$ . Constraints on low-mass Population III are weaker, because their elemental yields are very similar to Population II stars. However, the ionizing emissivity of low-mass Population III stars does not significantly differ from Population II stars, and so they do little to ease the tension between reionization constraints and observations of star-forming galaxies at high redshift.

One possible way in which our chemical constraints can be evaded is by having an UV photon escape fraction close to 100% for Population III stars, thus dramatically enhancing the impact of Population III on reionization for a given amount of Population III star-formation (and corresponding heavy element production). However, in our fiducial model, the contribution of Population III stars to the hydrogen photoionization rate is low predominantly because their contribution to the cosmic SFR density is extremely low throughout the epoch of reionization. As a result, even an escape fraction of 100% does not increase their contribution to reionization beyond that of the Population II stars. Additionally, it is not clear what physical process could lead to such a dramatic increase of the escape fraction at higher redshifts (Ferrara & Loeb 2013).

Our work suggests that Population III stars probably do not resolve the tension between reionization constraints and the paucity of ionizing photons implied by the observed population of star-forming galaxies at high redshift. Looking forward, our model also predicts that relative abundance measurements in the highest redshift ( $z \sim 7-8$ ) QSOs, and possibly also GRBs, should begin to probe the era when the vestiges of Population III star-formation had a significant impact on DLA relative abundance patterns.

#### ACKNOWLEDGEMENTS

We acknowledge useful discussions with Nishita Desai, Kristian Finlator, Katherine Inskip, Khee-Gan Lee, J. Xavier Prochaska, Alberto Rorai, and Raffaella Schneider. JFH acknowledges generous support from the Alexander von Humboldt foundation in the context of the Sofja Kovalevskaja Award. The Humboldt foundation is funded by the German Federal Ministry for Education and Research.

#### REFERENCES

- Abel, T., Bryan, G. L., & Norman, M. L. 2002, *Science*, 295, 93
- Alvarez, M. A., Finlator, K., & Trenti, M. 2012, *ApJ*, 759, L38
- Barkana, R., & Loeb, A. 2001, *Phys. Rep.*, 349, 125
- Becker, G. D., & Bolton, J. S. 2013, ArXiv e-prints
- Becker, G. D., Bolton, J. S., Haehnelt, M. G., & Sargent, W. L. W. 2011, *MNRAS*, 410, 1096
- Becker, G. D., Sargent, W. L. W., Rauch, M., & Carswell, R. F. 2012, *ApJ*, 744, 91
- Bolton, J. S., & Haehnelt, M. G. 2007, *MNRAS*, 382, 325
- Cen, R. 2003, *ApJ*, 591, L5
- Chiu, W. A., & Ostriker, J. P. 2000, *ApJ*, 534, 507
- Choudhury, T. R., & Ferrara, A. 2005, *MNRAS*, 361, 577
- . 2006, *MNRAS*, 371, L55
- Cooke, R., Pettini, M., Steidel, C. C., Rudie, G. C., & Nissen, P. E. 2011, *MNRAS*, 417, 1534
- Daigne, F., Olive, K. A., Silk, J., Stoehr, F., & Vangioni, E. 2006, *ApJ*, 647, 773

- Daigne, F., Olive, K. A., Vangioni-Flam, E., Silk, J., & Audouze, J. 2004, *ApJ*, 617, 693
- de Avillez, M. A., & Mac Low, M.-M. 2002, *ApJ*, 581, 1047
- Dessauges-Zavadsky, M., Péroux, C., Kim, T.-S., D’Odorico, S., & McMahon, R. G. 2003, *MNRAS*, 345, 447
- Dopcke, G., Glover, S. C. O., Clark, P. C., & Klessen, R. S. 2011, *ApJ*, 729, L3
- Erb, D. K., Shapley, A. E., Pettini, M., Steidel, C. C., Reddy, N. A., & Adelberger, K. L. 2006, *ApJ*, 644, 813
- Fakhouri, O., Ma, C.-P., & Boylan-Kolchin, M. 2010, *MNRAS*, 406, 2267
- Fan, X., Carilli, C. L., & Keating, B. 2006a, *ARA&A*, 44, 415
- Fan, X., et al. 2006b, *AJ*, 132, 117
- Faucher-Giguère, C.-A., Lidz, A., Hernquist, L., & Zaldarriaga, M. 2008, *ApJ*, 688, 85
- Ferrara, A., & Loeb, A. 2013, *MNRAS*, 431, 2826
- Finlator, K., Oh, S. P., Özel, F., & Davé, R. 2012, *MNRAS*, 427, 2464
- Font-Ribera, A., et al. 2012, *ArXiv e-prints*
- Fontanot, F., Cristiani, S., & Vanzella, E. 2012, *MNRAS*, 425, 1413
- Fukugita, M., & Peebles, P. J. E. 2004, *ApJ*, 616, 643
- Gardner, J. P., Katz, N., Hernquist, L., & Weinberg, D. H. 1997, *ApJ*, 484, 31
- . 2001, *ApJ*, 559, 131
- Gunn, J. E., & Peterson, B. A. 1965, *ApJ*, 142, 1633
- Haardt, F., & Madau, P. 2012, *ApJ*, 746, 125
- Heger, A., & Woosley, S. E. 2002, *ApJ*, 567, 532
- Hinshaw, G., et al. 2012, *ArXiv e-prints*
- Hopkins, A. M., & Beacom, J. F. 2006, *ApJ*, 651, 142
- Hui, L., & Haiman, Z. 2003, *ApJ*, 596, 9
- Kauffmann, G., Colberg, J. M., Diaferio, A., & White, S. D. M. 1999, *MNRAS*, 303, 188
- Kuhlen, M., & Faucher-Giguère, C.-A. 2012, *MNRAS*, 423, 862
- Kulkarni, G., Rollinde, E., Hennawi, J. F., & Vangioni, E. 2013, *ApJ*, 772, 93
- Larson, D., et al. 2011, *ApJS*, 192, 16
- Leitherer, C., et al. 1999, *ApJS*, 123, 3
- Maeder, A., & Meynet, G. 1989, *A&A*, 210, 155
- Maiolino, R., et al. 2008, *A&A*, 488, 463
- Matteucci, F. 2012, *Chemical Evolution of Galaxies*
- Meiksin, A., & White, M. 2004, *MNRAS*, 350, 1107
- Miralda-Escudé, J., Haehnelt, M., & Rees, M. J. 2000, *ApJ*, 530, 1
- Mitra, S., Choudhury, T. R., & Ferrara, A. 2011, *MNRAS*, 413, 1569
- Mitra, S., Ferrara, A., & Choudhury, T. R. 2012, *MNRAS*, L1
- Mortlock, D. J., et al. 2011, *Nature*, 474, 616
- Nagamine, K., Springel, V., & Hernquist, L. 2004a, *MNRAS*, 348, 421
- . 2004b, *MNRAS*, 348, 435
- Nagamine, K., Wolfe, A. M., Hernquist, L., & Springel, V. 2007, *ApJ*, 660, 945
- Naoz, S., Noter, S., & Barkana, R. 2006, *MNRAS*, 373, L98
- Noterdaeme, P., et al. 2012, *A&A*, 547, L1
- Ouchi, M., et al. 2010, *ApJ*, 723, 869
- Pagel, B. E. J. 2009, *Nucleosynthesis and Chemical Evolution of Galaxies*
- Péroux, C., Dessauges-Zavadsky, M., D’Odorico, S., Kim, T.-S., & McMahon, R. G. 2007, *MNRAS*, 382, 177
- Pontzen, A., et al. 2008, *MNRAS*, 390, 1349
- Prochaska, J. X., Herbert-Fort, S., & Wolfe, A. M. 2005, *ApJ*, 635, 123
- Prochaska, J. X., Worseck, G., & O’Meara, J. M. 2009, *ApJ*, 705, L113
- Rafelski, M., Wolfe, A. M., Prochaska, J. X., Neeleman, M., & Mendez, A. J. 2012, *ApJ*, 755, 89
- Raskutti, S., Bolton, J. S., Wyithe, J. S. B., & Becker, G. D. 2012, *MNRAS*, 421, 1969
- Robertson, B. E., Ellis, R. S., Dunlop, J. S., McLure, R. J., & Stark, D. P. 2010, *Nature*, 468, 49
- Robertson, B. E., et al. 2013, *ApJ*, 768, 71
- Rollinde, E., Vangioni, E., Maurin, D., Olive, K. A., Daigne, F., Silk, J., & Vincent, F. H. 2009, *MNRAS*, 398, 1782
- Rorai, A., Hennawi, J. F., & White, M. 2013, *ArXiv e-prints*
- Salvadori, S., Schneider, R., & Ferrara, A. 2007, *MNRAS*, 381, 647
- Schaerer, D. 2002, *A&A*, 382, 28
- Schaye, J., Aguirre, A., Kim, T.-S., Theuns, T., Rauch, M., & Sargent, W. L. W. 2003, *ApJ*, 596, 768
- Simcoe, R. A., Sargent, W. L. W., & Rauch, M. 2004, *ApJ*, 606, 92
- Sokasian, A., Yoshida, N., Abel, T., Hernquist, L., & Springel, V. 2004, *MNRAS*, 350, 47
- Spergel, D. N., et al. 2003, *ApJS*, 148, 175
- Springel, V., & Hernquist, L. 2003, *MNRAS*, 339, 312
- Tinsley, B. M. 1980, *Fund. Cosmic Phys.*, 5, 287
- Trenti, M., Stiavelli, M., Bouwens, R. J., Oesch, P., Shull, J. M., Illingworth, G. D., Bradley, L. D., & Carollo, C. M. 2010, *ApJ*, 714, L202
- Turk, M. J., Abel, T., & O’Shea, B. 2009, *Science*, 325, 601
- Vázquez, G. A., & Leitherer, C. 2005, *ApJ*, 621, 695
- Venkatesan, A., Tumlinson, J., & Shull, J. M. 2003, *ApJ*, 584, 621
- Wise, J. H., Turk, M. J., Norman, M. L., & Abel, T. 2012, *ApJ*, 745, 50
- Wolfe, A. M., Gawiser, E., & Prochaska, J. X. 2005, *ARA&A*, 43, 861
- Woosley, S. E., & Weaver, T. A. 1995, *ApJS*, 101, 181
- Wyithe, J. S. B., & Loeb, A. 2003, *ApJ*, 588, L69
- Yoshida, N., Bromm, V., & Hernquist, L. 2004, *ApJ*, 605, 579